Chalcogenide Letters Vol. 20, No. 4, April 2023, p. 301 - 313

Effect of metal cations on the conductivity and interfacial stability of $Li_7P_3S_{10.7}Br_{0.3}$ sulfide solid-state electrolytes

J. H. Zhou[a], S. H. Cao[b,*], X. Y. Li[a], C. Y. Shen[a], M. Cong[b]
[a]*Huizhou Power Supply Bureau, Guangdong Power Grid Co., Ltd. Huizhou 516000, Guangdong, China*
[b]*Shandong Taikai High Voltage Switchgear Co., Ltd., Tai'an 271000, Shandong, China*

The development of sulfide solid electrolyte is limited by the interface instability with lithium metal and low ionic conductivity. In this work, the effects of doping SiS_2, SnS, ZnS and MnS on the ionic conductivity and interfacial stability of sulfide electrolytes are systematically investigated. The conductivity of $Li_7P_{2.9}Sn_{0.1}S_{10.7}Br_{0.3}$ solid electrolyte was as high as 1.67 mS cm^{-1}. Furthermore, it is found that the critical current density was proportional to the resistivity of the doping element. The critical current density of the electrolyte was significantly increased by electronically insulating Si doping, reaching 0.858 mA cm^{-2}.

(Received February 8, 2022; Accepted April 28, 2023)

Keywords: Ionic conductivity, Solid electrolyte interface, Metal-doping, Li dendrites

1. Introduction

Among various solid-state electrolyte materials, sulfide solid electrolytes have received extensive attention due to their high ionic conductivity, cold compaction, and high safety [1]. Meanwhile, lithium metal is considered as the most promising anode due to its abundant reserves, large capacity and low density [2]. Therefore, sulfide solid-state electrolyte lithium-ion batteries are promising candidates for future secondary battery development. However, the sulfide solid electrolytes are unstable with Li metal, and their inevitable side reactions induce the growth of lithium dendrites, thus resulting in internal short circuit, which limits their further application [3-5].

A viable solid electrolyte must meet the following requirements: (i) high ionic conductivity [6]; (ii) wide and stable electrochemical window [7]; and (iii) good interfacial compatibility with Li metal [8]. Element doping is a practical way to improve electrolyte performance on the basis of these requirements. For instance, doping Cl, Br, and I halogen elements into electrolyte can effectively improve the conductivity of Li ions while optimizing the chemical stability of the electrolyte [9-12]. In terms of interfacial stability, $Li_7P_3S_{11}$ (LPS) electrolyte has been shown to have good interfacial compatibility with Li metal. Although a passivation layer is formed at the electrolyte/electrode interface through redox reactions to prevent

* Corresponding author: caosh@sdtaikai.com
https://doi.org/10.15251/CL.2023.204.301

the continuous occurrence of side reactions, it also produces higher interfacial resistance, which reduces its ionic conductivity [13]. Ion transport channels in LPS sulfide solid electrolytes can be widened through doping. This effect can improve the Li ion transport rate of the electrolytes. Moreover, the composition of the electrolytes can be adjusted to enhance interfacial compatibility with the Li metal anode. The doping of elements such as Si, Sn, Zn and Mn also ameliorates the ionic conductivity and adjusts the composition of SEI film to reduce the impedance at the interface [14-17]. The component part of SEI usually includes Li_3P, Li_2S and other polysulfides [18, 19]. The composition of the electrolyte greatly influences the content of the SEI layer, which affects the deposition behavior of Li metal during charging and discharging. Given that lithium dendrites must pass through the SEI layer when penetrating the electrolyte, the SEI passivation layer plays a key role in suppressing the growth of lithium dendrites. Hence, Han et al. doped LiI into the $75Li_2S$-$25P_2S_5$ sulfide electrolyte to form a LiI-containing SEI layer. The best inhibitory effect on Li dendrites was obtained at the I content of 30% [20]. Some works used Li-In alloy instead of metallic Li to alleviate side reactions between the electrolyte and lithium anode [21]. There are several methods to establish a protective layer of lithium to reduce the side reactions between the electrolyte and Li metal interface [22]. Nevertheless, these methods usually increase the overall resistance of the batteries, and the interface protection layer is hard to cover uniformly. Therefore, promoting the uniform deposition of Li^+ by adjusting the components that constitute the SEI film is a wise strategy for suppressing the growth of Li dendrites. However, the current works have not systematically investigated the effect of metal cation-doped sulfide electrolytes on Li metal diffusion.

In this work, we focused on doping Si, Sn, Zn and Mn into sulfide electrolytes to form $Li_7P_{2.9}X_{0.1}S_{10.7}Br_{0.3}$ (X= Mn, Si, Sn and Zn) solid electrolytes and explored the effects of different heat treatment temperatures on electrolyte ionic conductivity and cycling stability. The $Li_7P_{2.9}Sn_{0.1}S_{10.7}Br_{0.3}$ solid electrolyte obtained the highest ionic conductivity of 1.67 mS cm^{-1} after heat-treated at 220 °C. However, the $Li_7P_{2.9}Si_{0.1}S_{10.7}Br_{0.3}$ solid electrolyte obtained the highest critical current density of 0.858 mA cm^{-2} and could be stably cycled for 1000 h at a current density of 0.2 mA cm^{-2}.

2. Experiment

2.1. Preparation of electrolyte

The powders of Li_2S (99.9%, Aladdin), P_2S_5 (99.9%, Aladdin), LiBr (99.9%, Alfa Aesar) and SnS (99.9%, Aladdin) were mixed at the molar ratio of 3.35:1.45:0.3:0.1 and ground into a fine powder by using a mortar and pestle in a glove box with Ar protection. Then, the powders were transferred into an Ar-filled zirconia pot with 14 zirconia balls (10 mm in diameter). The samples were mechanically milled by using a planetary ball mill at 510 rpm for 24 h. The resulting powders were then placed into a quartz tube and heated at 220 °C in an Ar atmosphere for 3 h to obtain the glass-ceramic electrolyte $Li_7P_{2.9}Sn_{0.1}S_{10.7}Br_{0.3}$ (LPSSnBr). We prepared solid electrolytes doped with different metals, namely, $Li_7P_{2.9}Zn_{0.1}S_{10.7}Br_{0.3}$ (LPSZnBr), $Li_7P_{2.9}Mn_{0.1}S_{10.7}Br_{0.3}$ (LPSMnBr), $Li_7P_{2.9}Si_{0.1}S_{10.7}Br_{0.3}$ (LPSSiBr), and $Li_7P_3S_{10.7}Br_{0.3}$ (LPSBr), as the control group.

2.2. Material characterization

The X-ray diffraction (XRD) measurement of electrolytes were obtained with a Bruker D2 phase analyzer (10 mA, 30 kV) and CuKα radiation from 10° to 70° (2 °/min). We performed Raman spectroscopy (Renishaw In Via, Gloucestershire, UK) to observe the structural units of the electrolyte by using a Raman spectrometer with an excitation wavelength of 488 nm. The EIS measurements were performed at frequencies from 0.1 Hz to 1 MHz by utilizing an electrochemistry workstation (Zahner IM6). Electrolyte morphology and microstructure were observed by using scanning electron microscopy (SEM, JSM-7610F).

2.3. Electrochemical properties

Solid electrolyte samples were electrochemically measured by using a NEWARE-CT4008 cell test instrument. A total of 150 mg of electrolyte powder was cold pressed at 380 MPa to prepare electrolyte pellets with the diameter of 10 mm and thickness of 0.8 mm. Li metal was installed at both ends of the electrolyte as blocking electrodes and cold-pressed at 120 MPa. The critical current density test was performed over the range of 0.1–1 mA cm^{-2}, and the time for each charge and discharge was 30 min with the step length of 0.05 mA cm^{-2}. The current density of the cyclic stability test was 0.2 mA cm^{-2}, and the charge-discharge time was 30 min.

3. Result and discussion

3.1 Structural analysis

The phase analysis was performed by XRD. Fig. 1a shows the XRD patterns of the as-prepared electrolytes under heat treatment at 190 °C. All samples exhibited amorphous morphology. When the heat treatment temperature is 220 °C, the electrolytes exhibit obvious diffraction peaks, which are consistent with the diffraction peak characteristics of the LPS fast ion conductor phase (Fig. 1b). All samples showed the same crystal phase, indicating that the doping of different metal elements did not change the crystal structure of the final product, and all electrolytes belonged to the LPS system. Fig. 1c demonstrates the XRD pattern of the electrolyte heat-treated at 250 °C, besides the characteristic peaks of LPS were observed, the diffraction peak of $Li_4P_2S_6$ was observed at 33°. This is due to the fact that the LPS structure is a metastable phase, which will transform into stable phase structure $Li_4P_2S_6$ at higher temperature. According to previous reports, LPS was a highly ionic conducting phase with a triclinic structure, whereas $Li_4P_2S_6$ was a low ionic conducting phase [23, 24]. The addition of metal elements and halides into the prepared electrolyte increases vacancies and lithium ions concentration, which is beneficial to the propagation of lithium ions [25, 26].

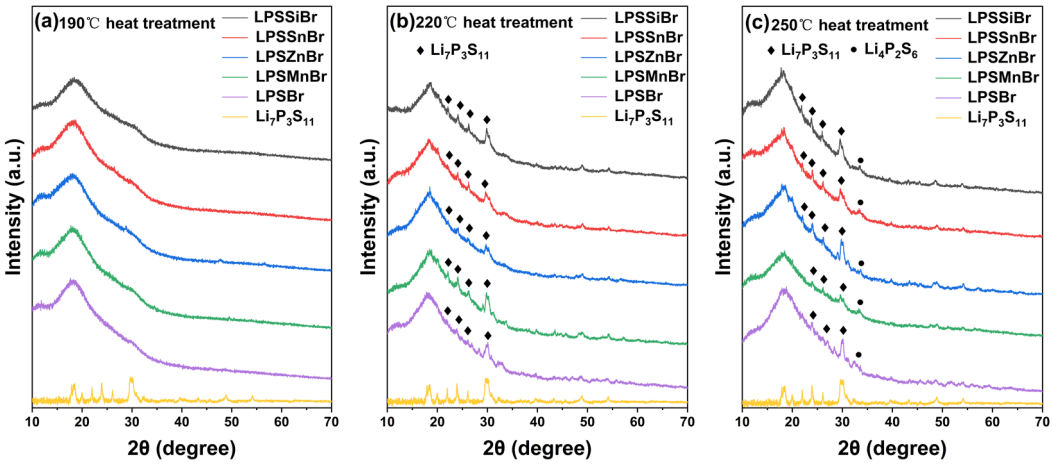

Fig. 1. X-ray diffraction pattern of the LPSSiBr, LPSSnBr, LPSZnBr, LPSMnBr and LPSBr solid electrolytes under (a) 190 °C, (b) 220 °C, (c) 250 °C heat treatment.

The ionic conductivities of all prepared sulfide electrolytes were calculated by electrochemical impedance spectroscopy (EIS) analysis. Fig. 2a–2c present the Nyquist plot of these metal doped solid electrolytes after heat treatment at different temperatures. The Nyquist plots for all electrolytes heat-treated at 190 °C and 250 °C (Figs. 2a and 2c) exhibit semicircular curves in the high frequency region, indicating high grain boundary resistance between the electrolyte particles. When heat-treated at 220 °C (Fig. 2b), the samples only present a tail at the medium and low frequency regions, indicating the existence of good interfacial contact with very low grain boundary/charge transfer resistance at the junction. In other words, as the heat treatment temperature was increased, the ionic conductivity of the samples first increased and then decreased (Fig. 2d). This behavior demonstrated that the heat treatment temperature had a significant effect on the ionic conductivity of the electrolyte. The optimal heat temperature is 220 °C for good grain boundary contact and ion transport between electrolyte particles. In particular, the Sn-doped LPSSnBr solid electrolyte reached the highest ionic conductivity of 1.67 mS cm^{-1} after heat treatment at 220 °C. In addition, the metal-doped electrolytes have higher ionic conductivity than that of the initial electrolytes after different heat treatment. This may be due to the replacement of P sites by metal elements, which broadened the ion transport channels and thus increasing the ionic conductivity. Xu et al. doped LPS electrolyte with MoS_2 and found that Mo ions replaced P to generate point defects, which expanded the ion transport channel. Not only that, Xu et al. also used Mn and I co-doping to obtain $Li_7P_{2.9}Mn_{0.1}S_{10.7}I_{0.3}$ glass-ceramic electrolytes and discovered that the large-sized metal cations effectively widened the ion transport path [15, 27].

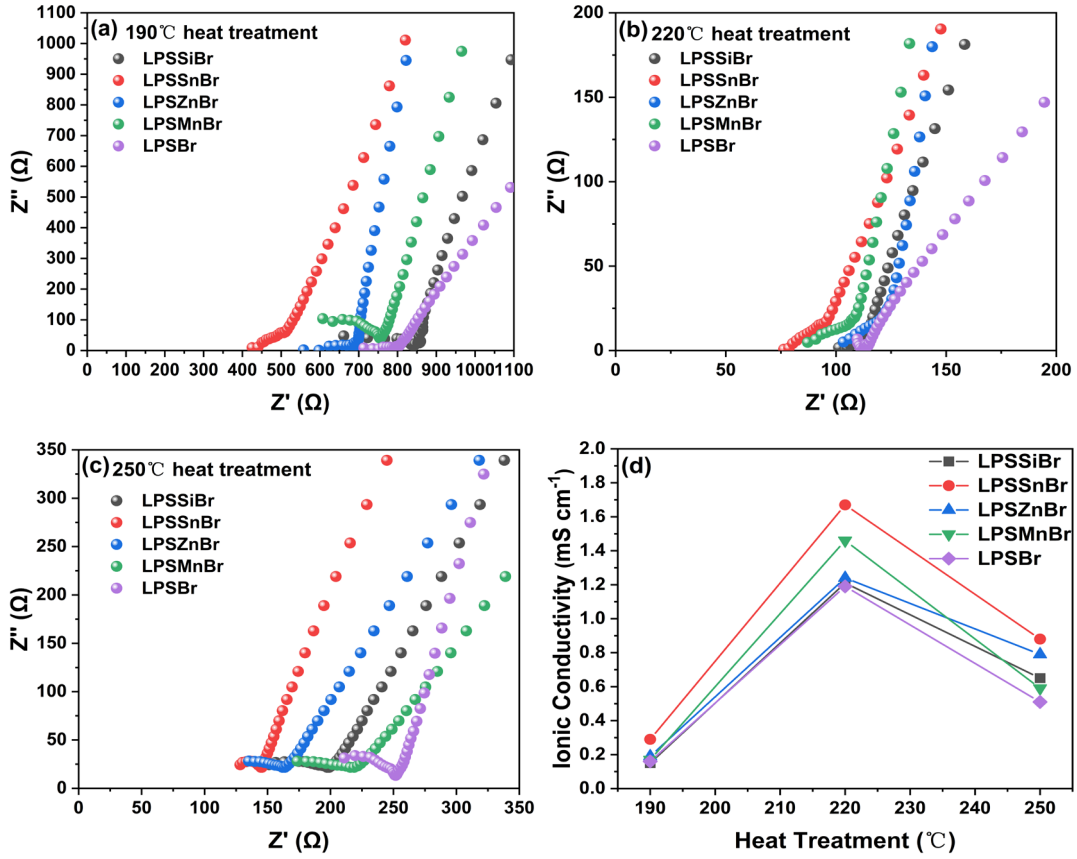

Fig. 2. EIS patterns of the LPSSiBr, LPSSnBr, LPSZnBr, LPSMnBr and LPSBr solid electrolytes at (a) 190 °C, (b) 220 °C, (c) 250 °C heat treatment. (d) conductivity of all the above electrolytes at different temperatures.

All the solid electrolytes prepared under heat treatment at 220 °C were tested. The wavelength range tested was between 300 and 500 cm^{-1}, as shown in Fig. 3. All samples exhibited two main peaks at 405 and 420 cm^{-1} that corresponded to the stretching of $P_2S_7^{4-}$ and PS_4^{3-}. The highly ionic conductive phase LPS also possessed $P_2S_7^{4-}$ and PS_4^{3-} functional groups [28, 29]. This result showed that the substitution of P by metal ions resulted in no change with the intensity ratio of the $P_2S_7^{4-}$ and PS_4^{3-} bands. It revealed that the main framework of metal-doped electrolyte was as the same as that of LPS, which is compatible with the XRD results.

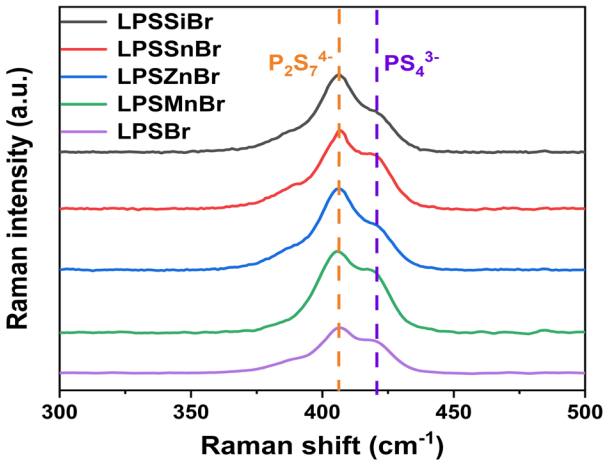

Fig. 3. Raman spectra of the LPSSiBr, LPSSnBr, LPSZnBr, LPSMnBr and LPSBr solid electrolytes after heat treatment at 220 °C.

Symmetric Li/electrolyte/Li cells were assembled to evaluate the ability to inhibit Li dendrite growth and the interfacial stability of metal-doped electrolytes against Li metal. Figs. 4a-4e provide the voltage versus current curves for metal-doped solid electrolytes. Initially, as the current density was increased, the voltage of the electrolyte increased. When the current was increased to a certain value, the voltage dropped suddenly. This voltage drop was considered to be the result of the penetration of lithium dendrites into the solid electrolyte, and the corresponding current density at the time of the voltage drop was regarded as the critical current density of the lithium dendrites piercing the electrolyte. Therefore, the ability to inhibit dendrite growth was evaluated on the basis of the critical current density [30, 31]. Fig. 4f compares the critical current densities of different metal-doped solid electrolytes. The critical current density of LPSSiBr, LPSSnBr, LPSZnBr, LPSMnBr, and LPSBr were 0.858, 0.468, 0.429, 0.546, and 0.624 mA cm^{-2}, respectively. The Si-doped electrolyte possessed lower ionic conductivity but had the highest critical current density, indicating that the doping of Si can suppress the penetration of lithium dendrites into the electrolyte. However, the critical current densities of Sn, Zn, and Mn doped electrolytes are lower than those of undoped electrolytes. Therefore, it can be known that the level of the ionic conductivity does not affect the critical current density.

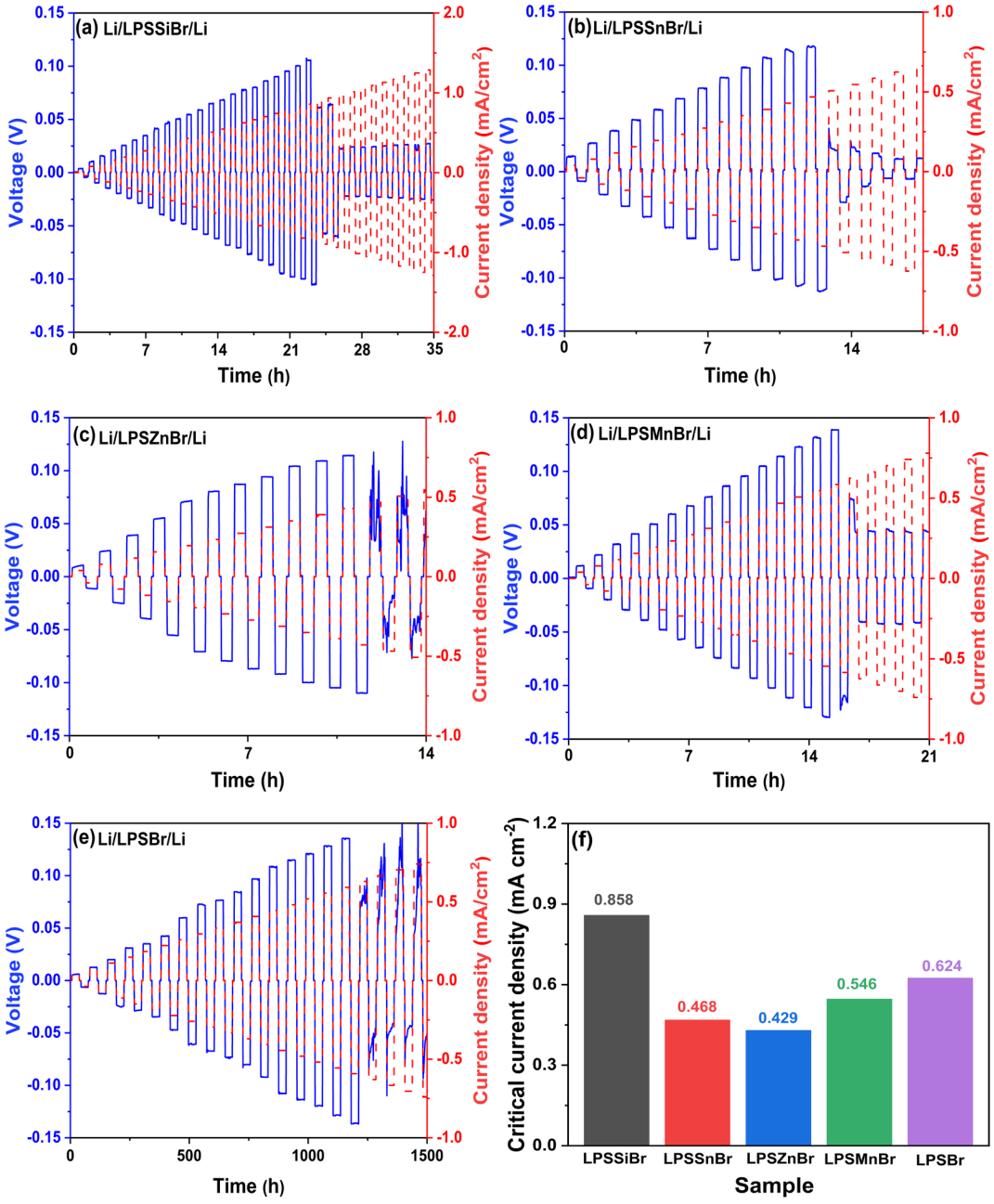

Fig. 4. Galvanostatic charge-discharge voltage profiles of (a) LPSSiBr, (b) LPSSnBr, (c) LPSZnBr, (d) LPSMnBr, (e) LPSBr. The time for each charge and discharge is 30 min, and the step size for the current increase is 0.05 mA cm^{-2}. (f) Critical current densities versus the composition of the sulfide electrolytes.

Previous studies have shown that both the electronic conductivity of the electrolyte and the interfacial reactions affect the critical current density of the assembled symmetric battery [32-34]. Fig. 5a demonstrates the direct current (DC) curves of the Li/electrolyte/Li cells at a bias voltage of 100 mV. Electronic conductivity was calculated by $\sigma_e=DI/SE$, D is the thickness of electrolyte, I is the current, S is the electrode area, and E represents voltage. The σ_e values of the five cells were 5.77×10^{-9}, 3.48×10^{-8}, 6.15×10^{-8}, 1.37×10^{-8} and 7.81×10^{-9} S cm^{-1}, respectively. By comparison,

it is found that when the electrolyte has a higher electronic conductivity, the corresponding critical current density is lower. As shown in Fig. 5b, as the resistivity of the dopant element increased, the critical current density of the electrolyte increased. In particular, given that Si is nonconductive, the LPSSiBr electrolyte had the best anti-lithium dendrite effect. If an electronic conductor is present in the SEI layer, electrons preferentially accumulate at the electronic conductor position during the battery charge-discharge cycle. This behavior results in uneven charge distribution and lithium deposition. Therefore, the doping of high-resistivity elements is highly favorable for restraining the growth of lithium dendrites in the electrolytes.

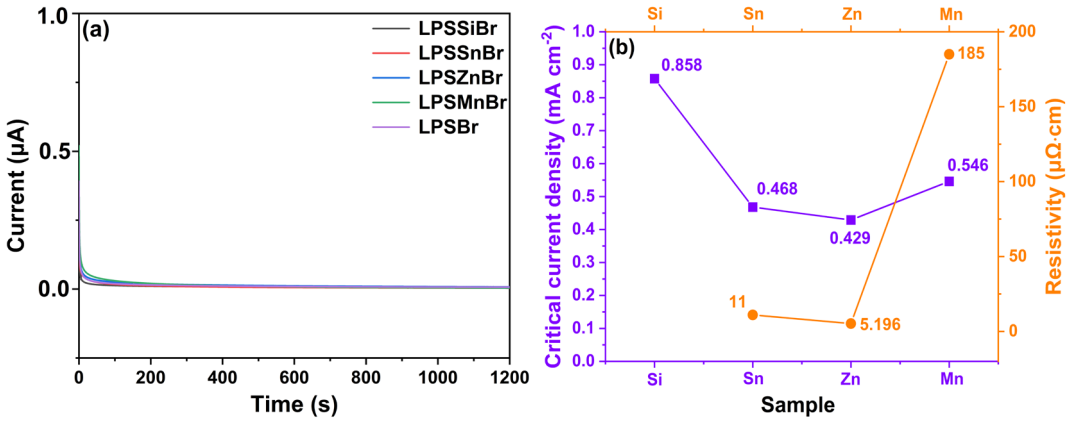

Fig. 5. (a) Current-time curves of In/LPSSiBr/In, In/LPSSnBr/In, In/LPSZnBr/In, In/LPSMnBr/In and In/LPSBr/In cells under DC polarization at 100 mV. (b) the critical current density of all prepared electrolytes and the resistivity of the doped metal element.

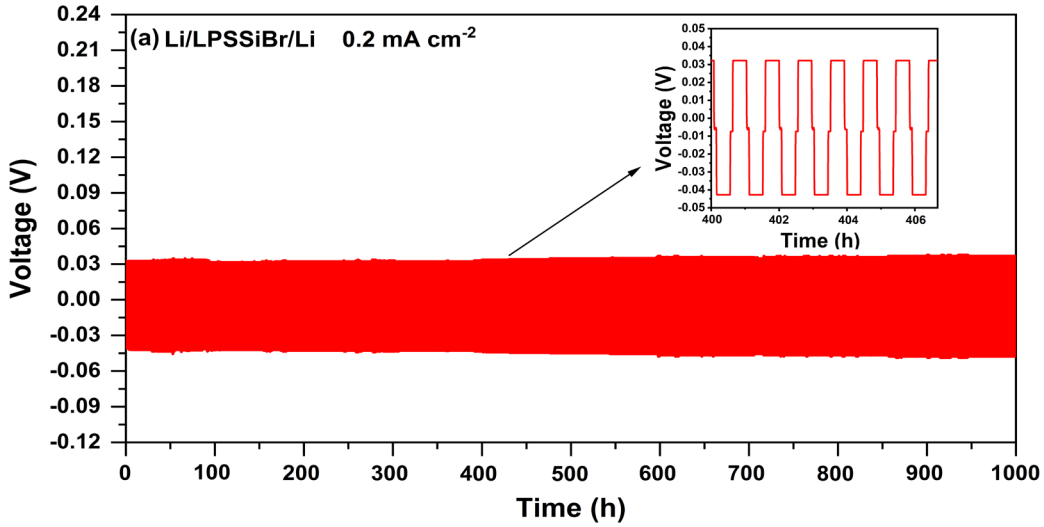

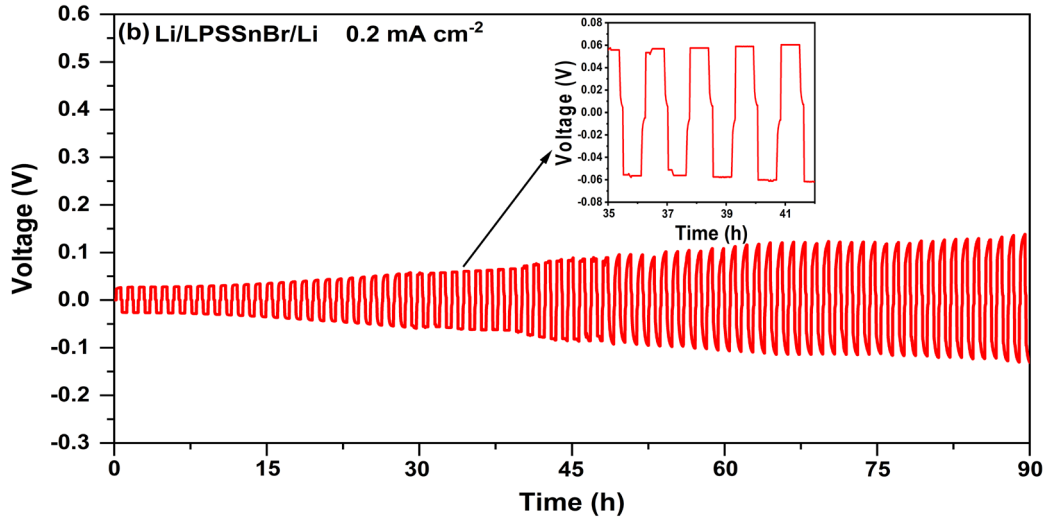
(b) Li/LPSSnBr/Li 0.2 mA cm-2
Voltage (V)
Time (h)
0.6
0.5
0.4
0.3
0.2
0.1
0.0
-0.1
-0.2
-0.3
0
15
30
45
60
75
90
0.08
0.06
0.04
0.02
0.00
-0.02
-0.04
-0.06
-0.08
35
37
39
41

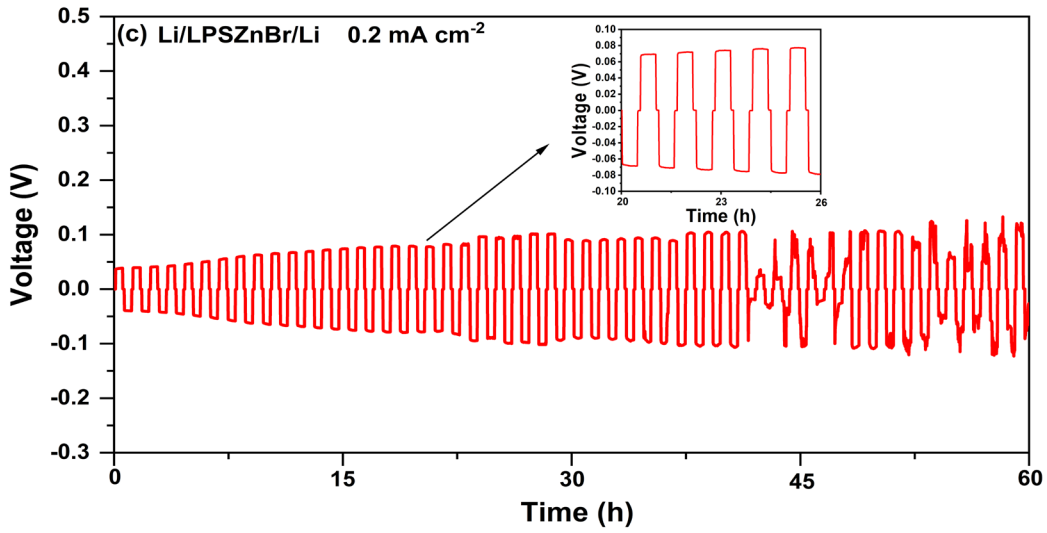
(c) Li/LPSZnBr/Li 0.2 mA cm-2
Voltage (V)
Time (h)
0.5
0.4
0.3
0.2
0.1
0.0
-0.1
-0.2
-0.3
0
15
30
45
60
0.10
0.08
0.06
0.04
0.02
0.00
-0.02
-0.04
-0.06
-0.08
-0.10
20
23
26

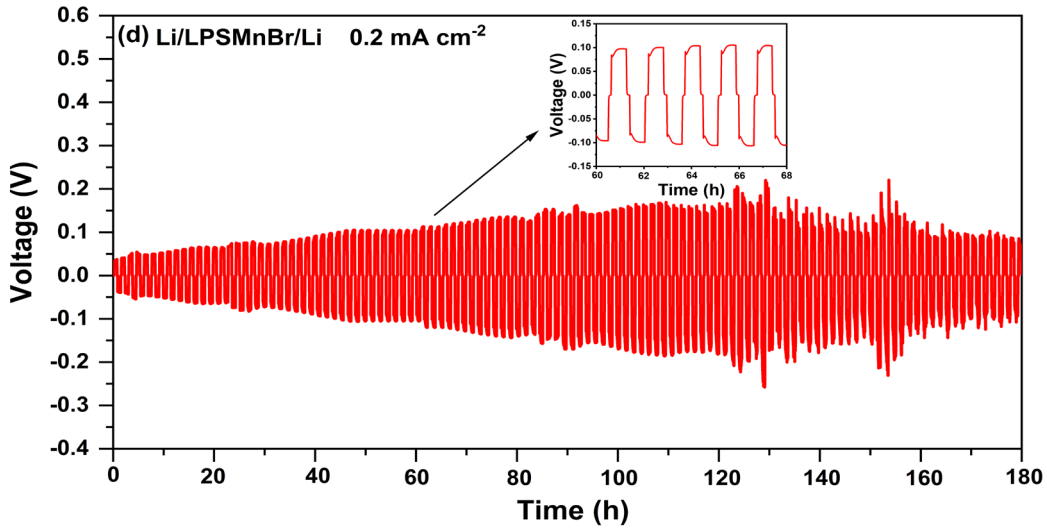
(d) Li/LPSMnBr/Li 0.2 mA cm-2
Voltage (V)
Time (h)
0.6
0.5
0.4
0.3
0.2
0.1
0.0
-0.1
-0.2
-0.3
-0.4
0
20
40
60
80
100
120
140
160
180
0.15
0.10
0.05
0.00
-0.05
-0.10
-0.15
60
62
64
66
68

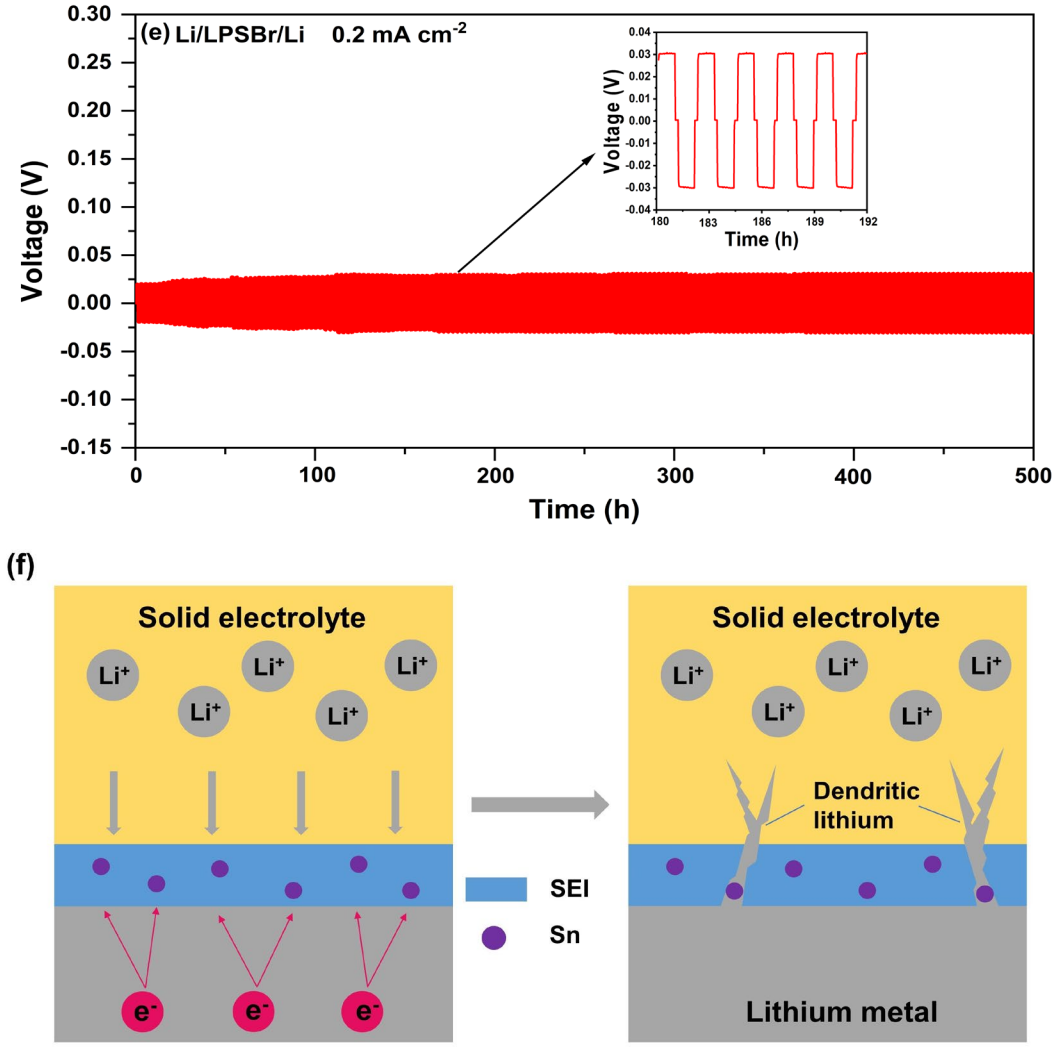

Fig. 6. Galvanostatic charge-discharge cycling profiles of (a) LPSSiBr, (b) LPSSnBr, (c) LPSZnBr, (d) LPSMnBr, (e) LPSBr. (f) Schematic of the growth behavior of lithium dendrites in LPSSnBr electrolyte.

The long cycling performance of symmetric cells was then compared with that of different metal cation doped electrolytes. Fig. 6a reveals the voltage curve of the Li/LPSSiBr/Li cell cycled at 0.2 mA cm^{-2}. The battery could be charged and discharged stably for up to 1000 h. Its cycle voltage stabilized at 0.03 V, indicating that a stable SEI layer had formed, which effectively inhibited Li dendrites. Fig. 6b demonstrates the voltage curve of the Li/LPSSnBr/Li cell cycled at 0.2 mA cm^{-2}. As the galvanostatic cycling progressed, the polarization voltage of the symmetric cell continuously increased, which was mainly due to the side reactions at the electrolyte/electrode interface. The continuous growth of SEI layer was caused by the continuous consumption of lithium by the side reactions, resulting in the increase in interfacial resistance. The battery died when the interface resistance had increased to a certain extent. The long cycling of the Li/LPSZnBr/Li cell at the current density of 0.2 mA cm^{-2} is shown in Fig. 6c. After 38 h, the polarization voltage dropped and the curve became unstable, which was due to the growth of lithium dendrites penetrating the electrolyte. Under the constant current cycle, the polarization

voltage of the Li/LPSMnBr/Li symmetrical battery increased continuously (Fig. 6d). The voltage became unstable after 100 h due to the short circuit induced by the infiltration of Li dendrites into the electrolyte. The non-zero voltage was indicative of the non-zero resistance of the dendrites. However, the electrolyte without metal cation elements was stably cycled for 500 h at the current density of 0.2 mA cm^{-2}. This result further proved that the doping of electronically conductive metal element was detrimental to the stability of the interface. Clearly, the Sn element in the SEI layer was formed after SnS was doped into the electrolyte as shown in Fig. 6f. Sn induced the aggregation of electrons by acting as an electron conductor. As a result, a large amount of Li was deposited on the Sn sites, resulting in non-uniform lithium accumulation. Therefore, the SEI layer formed by the electronically conductive metal cation-doped electrolyte is not beneficial to the diffusion and uniform deposition of Li^+.

4. Conclusion

In this work, the performance of sulfide solid-state electrolyte doped with SiS_2, SnS, ZnS and MnS was systematically studied. After 3 h of heat treatment at 220 °C, metal cation-doped electrolytes maintained the highly conductive phase structure of LPS. Among them, the ionic conductivity of the LPSSnBr electrolyte reached 1.67 mS cm^{-1}. However, this result did not imply an improvement in the interfacial stability of the cell. Although LPSBr electrolyte had lower ionic conductivity than the other electrolytes, its critical current density and long cycle performance were only inferior to LPSSiBr. This is mainly because Sn, Zn and Mn, by acting as electronic conductors, resulted in the non-uniform accumulation of Li ions, thus facilitating the growth of Li dendrites. The doping of electronically insulated Si inhibits the growth of Li dendrites. This effect was beneficial to cycling stability. This work provides a new route for the improvement of ionic conductivity in sulfide electrolyte and the formation of electrolyte stable passivation layer.

References

[1] W. Zhao, J. Yi, P. He, H. Zhou, Electrochem. Energy R. 2, 574-605 (2019); https://doi.org/10.1007/s41918-019-00048-0

[2] P. Albertus, S. Babinec, S. Litzelman, A. Newman, Nat. Energy 3, 16-21 (2017); https://doi.org/10.1038/s41560-017-0047-2

[3] J. Zheng, P. Yan, D. Mei, M.H. Engelhard, S.S. Cartmell, B.J. Polzin, C. Wang, J.G. Zhang, W. Xu, Adv. Energy Mater. 6, 1502151 (2016); https://doi.org/10.1002/aenm.201502151

[4] J. Li, C. Ma, M. Chi, C. Liang, N.J. Dudney, Adv. Energy Mater. 5, 1401408 (2015); https://doi.org/10.1002/aenm.201401408

[5] J. Janek, W.G. Zeier, Nat. Energy 1, 16141 (2016); https://doi.org/10.1038/nenergy.2016.141

[6] T. Matsuyama, M. Deguchi, A. Hayashi, M. Tatsumisago, T. Ozaki, Y. Togawa, S. Mori, Electrochemistry 83, 889-893 (2015); https://doi.org/10.5796/electrochemistry.83.889

[7] Noriaki, Kamaya, Kenji, Homma, Yuichiro, Yamakawa, Masaaki, Hirayama, Ryoji, Kanno, Nat. Mater. 10, 682-686 (2011); https://doi.org/10.1038/nmat3066

[8] M.R. Busche, D.A. Weber, Y. Schneider, C. Dietrich, S. Wenzel, T. Leichtweiss, D. Schröder, W. Zhang, H. Weigand, D. Walter, S.J. Sedlmaier, D. Houtarde, L.F. Nazar, J. Janek, Chem. Mater. 28, 6152-6165 (2016); https://doi.org/10.1021/acs.chemmater.6b02163

[9] Z. Zhu, I.H. Chu, S.P. Ong, Chem. Mater. 6, 2474-2484 (2016); https://doi.org/10.1021/acs.chemmater.6b04049

[10] N. Zhang, F. Ding, S. Yu, K. Zhu, H. Li, W. Zhang, X. Liu, Q. Xu, ACS Appl. Mater. Interfaces 11, 27897-27905 (2019); https://doi.org/10.1021/acsami.9b08218

[11] E. Rangasamy, Z. Liu, M. Gobet, K. Pilar, G. Sahu, W. Zhou, W. Hui, S. Greenbaum, C. Liang, J. Am. Chem. Soc 46, 1384-1387 (2014); https://doi.org/10.1021/ja508723m

[12] S.J. Choi, S.H. Choi, A.D. Bui, Y.J. Lee, S.M. Lee, H.C. Shin, Y.C. Ha, ACS Appl. Mater. Interfaces 10, 31404-31412 (2018); https://doi.org/10.1021/acsami.8b11244

[13] K.H. Park, Q. Bai, D.H. Kim, D.Y. Oh, Y. Zhu, Y. Mo, Y.S. Jung, Adv. Energy Mater. 8, 1800035 (2018); https://doi.org/10.1002/aenm.201800035

[14] T. Chen, L. Zhang, Z. Zhang, P. Li, H. Wang, C. Yu, X. Yan, L. Wang, B. Xu, ACS Appl. Mater. Interfaces 11, 40808-40816 (2019); https://doi.org/10.1021/acsami.9b13313

[15] R. Xu, X. Xia, S. Li, S. Zhang, X. Wang, J. Tu, J. Mater. Chem. A 5, 6310-6317 (2017); https://doi.org/10.1039/C7TA01147D

[16] M. Murayama, J. Solid State Chem. 168, 140-148 (2002); https://doi.org/10.1006/jssc.2002.9701

[17] T. Kaib, S. Haddadpour, M. Kapitein, P. Bron, C. Schröder, H. Eckert, B. Roling, S. Dehnen, Chem. Mater. 24, 2211-2219 (2012); https://doi.org/10.1021/cm3011315

[18] S. Wenzel, D.A. Weber, T. Leichtweiss, M.R. Busche, J. Sann, J. Janek, Solid State Ionics 286, 24-33 (2016); https://doi.org/10.1016/j.ssi.2015.11.034

[19] Z. Wang, Y. Jiang, J. Wu, Y. Jiang, W. Ma, Y. Shi, X. Liu, B. Zhao, Y. Xu, J. Zhang, Nano Energy 84, 105906 (2021); https://doi.org/10.1016/j.nanoen.2021.105906

[20] F. Han, J. Yue, X. Zhu, C. Wang, Adv. Energy Mater. 8, 1703644 (2018); https://doi.org/10.1007/978-981-13-0158-2

[21] N. Ohta, K. Takada, L. Zhang, R. Ma, M. Osada, T. Sasaki, Adv. Mater. 18, 2226-2229 (2006); https://doi.org/10.1002/adma.200502604

[22] C. Wang, Y. Zhao, Q. Sun, X. Li, Y. Liu, J. Liang, X. Li, X. Lin, R. Li, K.R. Adair, L. Zhang, R. Yang, S. Lu, X. Sun, Nano Energy 53, 168-174 (2018); https://doi.org/10.1016/j.nanoen.2018.08.030

[23] C. Park, S. Lee, M. Kim, Electrochim. Acta 390, 138808 (2021); https://doi.org/10.1016/j.electacta.2021.138808

[24] X. Xu, G. Hou, X. Nie, Q. Ai, Y. Liu, J. Feng, L. Zhang, P. Si, S. Guo, L. Ci, J. Power Sources 400, 212-217 (2018); https://doi.org/10.1016/j.jpowsour.2018.08.016

[25] I.H. Chu, H. Nguyen, S. Hy, Y.C. Lin, Z. Wang, Z. Xu, Z. Deng, Y.S. Meng, S.P. Ong, ACS Appl. Mater. Interfaces 8, 7843-7853 (2016); https://doi.org/10.1021/acsami.6b00833

[26] H. Yamane, M. Shibata, Y. Shimane, T. Junke, Y. Seino, S. Adams, K. Minami, A. Hayashi, M. Tatsumisago, Solid State Ionics 178, 1163-1167 (2007); https://doi.org/10.1016/j.ssi.2007.05.020

[27] R. Xu, X. Xia, X. Wang, Y. Xia, J. Tu, J. Mater. Chem. 5, 2829-2834 (2017); https://doi.org/10.1039/C6TA10142A

[28] J. Wei, H. Kim, D. Lee, R. Hu, F. Wu, H. Zhao, F.M. Alamgir, G. Yushin, J. Power Sources 294, 494-500 (2015); https://doi.org/10.1016/j.jpowsour.2015.06.074

[29] S. Ito, M. Nakakita, Y. Aihara, T. Uehara, N. Machida, J. Power Sources 271, 342-345 (2014); https://doi.org/10.1016/j.jpowsour.2014.08.024

[30] A. Sharafi, H.M. Meyer, J. Nanda, J. Wolfenstine, J. Sakamoto, J. Power Sources 302, 135-139 (2016); https://doi.org/10.1016/j.jpowsour.2015.10.053

[31] C.L. Tsai, V. Roddatis, C.V. Chandran, Q. Ma, S. Uhlenbruck, M. Bram, P. Heitjans, O. Guillon, ACS Appl. Mater. Interfaces 8, 10617-10626 (2016); https://doi.org/10.1021/acsami.6b00831

[32] F. Han, A.S. Westover, J. Yue, X. Fan, F. Wang, M. Chi, D.N. Leonard, N.J. Dudney, H. Wang, C. Wang, Nat. Energy 4, 187-196 (2019); https://doi.org/10.1038/s41560-018-0312-z

[33] F. Mo, J. Ruan, S. Sun, Z. Lian, S. Yang, X. Yue, Y. Song, Y.N. Zhou, F. Fang, G. Sun, S. Peng, D. Sun, Adv. Energy Mater. 9, 1970155 (2019); https://doi.org/10.1002/aenm.201970155
[34] R. Raj, J. Wolfenstine, J. Power Sources 343, 119-126 (2017); https://doi.org/10.1016/j.jpowsour.2017.01.037